

# PCCP

Accepted Manuscript



This is an *Accepted Manuscript*, which has been through the Royal Society of Chemistry peer review process and has been accepted for publication.

*Accepted Manuscripts* are published online shortly after acceptance, before technical editing, formatting and proof reading. Using this free service, authors can make their results available to the community, in citable form, before we publish the edited article. We will replace this *Accepted Manuscript* with the edited and formatted *Advance Article* as soon as it is available.

You can find more information about *Accepted Manuscripts* in the [Information for Authors](#).

Please note that technical editing may introduce minor changes to the text and/or graphics, which may alter content. The journal's standard [Terms & Conditions](#) and the [Ethical guidelines](#) still apply. In no event shall the Royal Society of Chemistry be held responsible for any errors or omissions in this *Accepted Manuscript* or any consequences arising from the use of any information it contains.

# CO<sub>2</sub> Conversion to Methanol on Cu(I) Oxide Nanolayers and Clusters: Electronic Structure Insight into the Reaction Mechanism

*Ellie L. Uzunova<sup>a</sup>, Nicola Seriani<sup>b</sup>, Hans Mikosch<sup>c</sup>*

<sup>a</sup> Institute of General and Inorganic Chemistry, Bulgarian Academy of Sciences, Acad. G. Bonchev Str., bl. 11, Sofia 1113, Bulgaria; <sup>b</sup> Abdus Salam International Centre for Theoretical Physics, Condensed Matter and Statistical Physics Section, Strada Costiera 11, 34151 Trieste, Italy;

<sup>c</sup> Institute for Chemical Technologies and Analytics, Vienna University of Technology, Getreidemarkt 9/E164/EC, A-1060 Vienna, Austria

ellie@svr.igic.bas.bg

## ABSTRACT

The mechanism of carbon dioxide reduction to methanol on Cu(I) oxide nanolayers and clusters using water as a source of hydrogen was traced by density functional theory. The nature of the active sites is revealed, namely the role of surface copper dimers, which are present on the Cu<sub>2</sub>O(001) surface and in the nanoclusters of size Cu<sub>32</sub>O<sub>16</sub> and Cu<sub>14</sub>O<sub>7</sub>. The major difference between metal catalysts and Cu<sub>2</sub>O is outlined: the CO<sub>2</sub> molecule interacts strongly with the oxide and undergoes bending prior to hydrogenation. The first step of CO<sub>2</sub> hydrogenation results in the formation of a stable carboxyl intermediate, -CO(OH), which in the following steps is converted to methanol via formic acid and formaldehyde intermediates. The consumption of hydrogen from water leaves

surface peroxy- and hydroperoxy- species. The peroxides easily desorb molecular oxygen, while for hydroperoxides the reaction of oxygen evolution requires activation energy of  $130 \text{ kJ mol}^{-1}$ . The maxima in absorption spectra correspond well with the required activation energies in the elementary steps.

Keywords: Carbon Dioxide Activation, water dissociation, Methanol,  $\text{Cu}_2\text{O}$ , reaction mechanism of  $\text{CO}_2$  hydrogenation

## INTRODUCTION

The carbon dioxide utilization has become a major challenge in research and the search for efficient catalysts to produce either feedstock for the chemical industry or fuel (methanol, methane) marked significant progress in the recent years. Still, there are not many industrial processes to use CO<sub>2</sub> as raw material, because as the final product of fuel combustion it is an endothermic compound and relatively inert. The relatively high reduction potential (1.9 V to CO<sub>2</sub><sup>-</sup>) can be lowered if the reduction targets hydrogenated products.<sup>1</sup> With the exception of polymerization reactions to polycarbonates and the synthesis of carbamates, all routes to utilize CO<sub>2</sub> are hydrogenative. The hydrogen, needed as reactant, can be produced in a preliminary electrochemical or photoelectrochemical step of water splitting, but a great advantage would be the direct use of water in the reduction of CO<sub>2</sub>. In the recent years, significant steps forward have been made in this direction: methane has been produced on a Cu/TiO<sub>2</sub> (titania nanotube) photocatalyst under solar energy from CO<sub>2</sub> and water;<sup>2</sup> CuO-Cu<sub>2</sub>O nanorods have been used as a photoelectrocatalyst to produce methanol;<sup>3</sup> direct photocatalytic reduction of CO<sub>2</sub> to CO using water as reagent was achieved on amorphous copper oxide nanoclusters grafted on niobate nanosheets.<sup>4</sup> A vast number of studies explored copper-based catalysts, which certainly include the industrial Cu/ZnO/Al<sub>2</sub>O<sub>3</sub> catalyst for methanol production from syngas, CO/CO<sub>2</sub>/H<sub>2</sub>.<sup>5-12</sup> The reaction mechanism of CO and CO<sub>2</sub> hydrogenation on metal surfaces was subject of detailed theoretical studies.<sup>7-11</sup> The structures of reaction intermediate species were determined by density functional theory (DFT) calculations<sup>7-10</sup> and some of the proposed intermediates have been detected experimentally, e.g. formate and carboxylate.<sup>9</sup> The understanding of the reaction mechanism is essential for improving catalytic performance, but most of our knowledge at present is limited to metal surfaces and layers, while oxides were mainly examined with respect to water splitting and R–OH bond-breaking, (R=H, CH<sub>3</sub>, C<sub>2</sub>H<sub>5</sub>).<sup>12-19</sup> It is worth noting, that many of the known oxide photocatalysts, electrocatalysts or co-catalysts consist of nanoclusters, grafted on a semiconductor or another support, and the active phase

does not consist of crystallites, but is in fact amorphous.<sup>4,12,20</sup> The experimental methods provide scarce information on the elementary building blocks of such materials. In the search of efficient catalysts for the reduction of carbon dioxide to fuel (CO, hydrocarbons, methanol) capable in using solar energy to promote the reaction, cuprous oxide (Cu<sub>2</sub>O) has been considered a relevant candidate, based on its favorable band gap position and width.<sup>21</sup> As a photocatalyst for water splitting Cu<sub>2</sub>O did not gain great success, since oxidation to CuO and trapping effect from defect sites occurred, but proved more efficient in reduction reactions as photocathode.<sup>13</sup> At high oxygen pressure, copper vacancies are responsible for the p-type conductivity of cuprous oxide, thus most of the theoretical studies have been focused on copper vacancies in bulk structures and copper-deficient surface terminations.<sup>22</sup> From experimental studies it is known, that the Cu<sub>2</sub>O (001) surface can be prepared oxygen-rich, or copper-rich, with various reconstructions, depending on oxygen pressure and annealing conditions.<sup>23-25</sup> Therefore, we have examined Cu<sub>2</sub>O (001) as polar copper terminated surface and also as oxygen-terminated surface, using density functional theory (DFT) with periodic boundary conditions (PBC). The active sites for water adsorption and dissociation, as well as for CO<sub>2</sub> adsorption, activation and reduction were sought on copper-terminated and oxygen-terminated nanolayers of thickness corresponding to four [Cu<sub>2</sub>O] bi-layers, and finite cluster models of size Cu<sub>32</sub>O<sub>16</sub> and Cu<sub>14</sub>O<sub>7</sub>; in the CO<sub>2</sub> hydrogenation reaction path following the smaller size Cu<sub>14</sub>O<sub>7</sub> cluster was used. As water dissociation towards surface hydroxyls (H-OH bond breaking) proved to have minor energy barrier on both nanolayers and clusters, water has been considered as a source of hydrogen for the CO<sub>2</sub> reduction.

## Methods

The periodic calculations of crystalline solid Cu<sub>2</sub>O and Cu<sub>2</sub>O nanolayers were performed with the range separated hybrid density functional HSE06<sup>26</sup> implemented in Gaussian 09,<sup>27</sup> using a (10,10,10) k-point mesh for the three-dimensional calculations of the bulk oxide (3D models) and

(20,20,0) for the nanolayer models. Eight  $\text{Cu}_2\text{O}$  unit cells are included explicitly in all periodic calculations. The B3LYP density functional, which includes local and non-local terms,<sup>28</sup> and HSE06 (for comparison with periodic calculations) have been applied in cluster studies. The minima on the potential energy surfaces were identified by the absence of negative eigenvalues in the diagonalized Hessian matrix; transition states were characterized by the presence of a single imaginary frequency. Time-dependent (TD) DFT was used<sup>29</sup> to determine the UV-VIS absorption spectra of the  $\text{Cu}_{14}\text{O}_7$  clusters and their adsorption complexes with  $\text{CO}_2$ . The synchronous transit-guided quasi-Newton (STQN) method was used for the transition state optimizations.<sup>30</sup> Dispersion effects were taken into account by using the empirical formula of Grimme.<sup>31</sup> The bond populations and charge distributions were examined by natural bond orbital (NBO) analysis.<sup>32</sup> More details on the computational methods and basis sets used, as well as the method validation are presented as Supplementary Information.

### Structure and Bonding of $\text{Cu}_2\text{O}$ : The Crystalline oxide, Nanolayer and Clusters

*Crystalline oxide and Nanolayers.* Nanoclusters are the active component of photo- and electrocatalysts, either grafted on another material, or as a separate phase, so a major question arises whether they would inherit elements of the crystal surface reconstructions. The simple cubic structure of cuprite ( $\text{Cu}_2\text{O}$ , space group  $\text{Pn}\bar{3}\text{m}$ , No. 224) can be viewed as two sublattices: a face-centered cubic (fcc) sublattice of copper cations and a body-centered cubic (bcc) sublattice of oxygen anions.<sup>33</sup> The oxygen anions are tetrahedrally coordinated by copper cations, while each copper center is part of linear  $-\text{O}-\text{Cu}-\text{O}-$  groups, formed with the two nearest oxygen neighbors, Figure 1. It is a peculiar feature of cuprite, that oxygen has a higher coordination number than the transition metal cation. The properties of the bulk solid are correctly reproduced by our calculations, Table 1. A number of surface reconstructions have been reported experimentally and studied by first principle methods.<sup>17,23,34</sup> On the polar copper-terminated surface, the (1×1) row-missing

reconstruction has been found as the most stable one by calculations using Buckingham type potentials.<sup>17</sup> Experimentally, a weak  $(3\sqrt{2}\times\sqrt{2})R45^\circ$  pattern with many missing spots and two variants at  $90^\circ$  have been reported by Low Energy Electron Diffraction (LEED).<sup>23</sup> On the copper-terminated surface of  $\text{Cu}_2\text{O}$ , built of  $4[\text{Cu}_2\text{O}]$  bi-layers, oxygen atoms remain as centers of distorted tetrahedra, while copper atoms pull together and Cu(I)-Cu(I) bonds of lengths in the range 2.18-2.94 Å are created, Figure 1c. Stabilization of the surface is achieved by formation of Cu(I)-Cu(I) surface dimers and Cu(I)-Cu(I) bonds are also formed between the surface layer and the first inner Cu-layer. The surface dimers of bond length 2.184 Å lie in the [110] plane, while the bonds with Cu(I) cations from the inner layer contribute to a larger four-membered copper assembly. The 2.408 Å and 2.938 Å Cu(I)-Cu(I) internuclear distances, formed with inner-layer cations, calculated in our work agree with the values reported in previous studies (2.516 Å; 3.039 Å), but the Cu(I)-Cu(I) internuclear distance in the surface dimer is shorter, 2.184 Å from HSE06 vs 2.401 Å (GGA) or 2.374 (LDA).<sup>34</sup> The oxygen terminated surface also contains Cu(I)-Cu(I) dimers with internuclear distances of 2.478 Å, Figure 1d. The angle OCuO near the surface is no longer linear, but bends to  $164.5^\circ$ . The Cu-O terminal bonds are considerably shorter, 1.721 Å, compared to other Cu(I)-O bonds, also those in finite  $\text{Cu}_2\text{O}$  clusters.

*Nanoclusters.* In the formation of  $\text{Cu}_{32}\text{O}_{16}$  clusters a cut-off consisting of eight  $\text{Cu}_2\text{O}$  unit cells was allowed to fully relax; a three-layer four-cell cut-off was used for the  $\text{Cu}_{14}\text{O}_7$  model. These clusters contain elements from the bulk  $\text{Cu}_2\text{O}$  crystal structure: linear O-Cu-O bonds and tetrahedrally coordinated oxygen atoms. The elements of the  $\text{Cu}_2\text{O}$  surface reconstruction include surface Cu(I)-Cu(I) dimers, which form bonds with inner Cu(I) cations to set-up larger assemblies, Figure 2S, Supplementary Information. The Cu(I)-Cu(I) bonds fall into the range of lengths 2.264 – 2.353 Å for  $\text{Cu}_{32}\text{O}_{16}$ ; for the smaller cluster this range is similar, slightly shifted to longer bonds of 2.366 – 2.477 Å, Table 1. Natural population analysis reveals significant covalent character of the Cu(I)-Cu(I) and

Cu(I)-O bonds, Table 2. The partial charge on copper centers does not exceed 0.77 e, while the negative charge on oxygen centers varies within the range  $-1.07 \div -1.33$  e. The Cu 4s orbital is significantly populated which enables the formation of highly delocalized bonding orbitals via 3d-4s hybridization.

### Adsorption and Dissociation of Water on Cu<sub>2</sub>O Nanolayers and Clusters

It is known from experiments that above 300 K, water adsorption on a Cu (001) surface is dissociative, while at lower temperatures, 110 K, dissociated and molecular water coexist.<sup>18,24</sup> The presence of coordinatively unsaturated oxygen atoms is essential for water molecule dissociation, and though the adsorption energies are quite similar for the copper-terminated or oxygen-terminated surface of Cu<sub>2</sub>O (001), 140 kJ mol<sup>-1</sup>, vs 144 kJ mol<sup>-1</sup>, our calculations predict that water dissociation is spontaneous only at the oxygen-terminated surface. The dissociation of water results in formation of closely positioned hydroxyl groups at the coordinatively unsaturated oxygen atoms. The Cu-Cu bonds in proximity to the dissociated water molecule are lengthened from 2.478 Å to 2.976 Å and the -OH group from the dissociated water molecule forms a bridging Cu-OH-Cu bond. We find a preferred position of molecular adsorption on top of a copper atom, whereas for the dissociative form our study points to a more stable structure with the hydroxyl group in a bridging position between two copper cations, (Figure 3S, Supplementary Information).

Several adsorption sites are available for water molecules on the Cu<sub>32</sub>O<sub>16</sub> cluster, with adsorption energies varying in the range 130 – 164 kJ mol<sup>-1</sup>. The most favorable adsorption sites for water dissociation on either Cu<sub>32</sub>O<sub>16</sub> or Cu<sub>14</sub>O<sub>7</sub> are copper sites among the copper atom assemblies. They bind the hydroxyl group resulting after the H-OH bond breaking ( $\text{H}_2\text{O} \Rightarrow \text{H}^*_{\text{surf}} + \text{OH}^*_{\text{surf}}$ ). The hydrogen becomes part of a bridging hydroxyl group Cu(OH)Cu by binding to a coordinatively unsaturated oxygen center. The solid crystalline Cu<sub>2</sub>O is capable to form hydroxyl groups in the inner layer and the lowest energy configurations resulting from diffusion of atomic hydrogen have

been subject of DFT studies<sup>14</sup>, which predicted a bond-centred interstitial hydroxyl and an inverted tripodal hydroxyl. These sites however, are less accessible and cannot serve as active sites for hydrogenation. According to our results, the coordinatively unsaturated oxygen centers at the surface of  $\text{Cu}_{32}\text{O}_{16}$  and  $\text{Cu}_{14}\text{O}_7$  ( $\text{Cu}_3\text{-O}$ ) have high proton affinity of  $1326 \text{ kJ mol}^{-1}$ , which makes them a preferred site for hydroxyl group formation. Upon dissociative water adsorption the  $\text{Cu(I)-Cu(I)}$  bonds are lengthened, more significantly at the nanolayer surface, whereas at the nanoclusters the change is much smaller, Table 3. The process of water dissociation proved to be practically barrier-free at the  $\text{Cu}_4$ -site of  $\text{Cu}_{14}\text{O}_7$ , as the calculated activation energy is only  $0.9 \text{ kJ mol}^{-1}$ .

### **$\text{CO}_2$ Adsorption and Hydrogenation on $\text{Cu}_2\text{O}$ Nanolayers and Clusters.**

The  $\text{CO}_2$  molecule can be adsorbed on  $\text{Cu}_2\text{O}$  either end-on, at copper sites, retaining its linear form, or by forming a surface carbonate at coordinatively unsaturated oxygen centers. The adsorption energy for binding via one oxygen atom of  $\text{CO}_2$  to a terminal copper atom of the  $\text{Cu}_{14}\text{O}_7$  cluster is  $88 \text{ kJ mol}^{-1}$ , and it is much lower at the  $\text{Cu}_2\text{O}(001)$  surface,  $48 \text{ kJ mol}^{-1}$ , where a bridging position between two copper cations is preferred. The formation of surface carbonate is achieved in the presence of neighboring oxygen and copper coordinatively unsaturated centers, at which the  $\text{CO}_2$  molecule binds via one oxygen atom and one carbon atom, Figure 2a. The redistribution of charges is minor, the surface oxygen which participates in the formation of  $\text{CO}_3^{2-}$  remains considerably ionic in nature, with a natural charge changing from -1.30 to -1.10; the copper center charge increases from +0.64 to +0.68. The oxygen of the C-O-Cu linkage bears a charge of -0.82, while the terminal oxygen atom of the  $\text{CO}_3^{2-}$  group has a local charge of -0.62. The adsorption energy of carbonate species reaches  $123 \text{ kJ mol}^{-1}$ . On a metallic copper surface the GGA-DFT calculated binding energy of carbonate was reported as much higher,  $350 \text{ kJ mol}^{-1}$ .<sup>7</sup> In presence of surface hydroxyls,  $\text{CO}_2$  adsorption at the copper assemblies occurs via bonding to two adjacent copper centers by forming Cu-O and Cu-C bonds, which results in strongly bent  $\text{CO}_2^{\delta-}$ , Figure 2b. The adsorption energy in this

case increases to  $240 \text{ kJ mol}^{-1}$  due to hydrogen-bond formation. In the first hydrogenation step the oxygen atom of  $\text{CO}_2$ , non-bonded to the surface, accepts hydrogen to form a carboxyl intermediate –  $\text{CO}(\text{OH})$ , Table 4. The calculated activation barrier to carboxyl formation is only  $13.8 \text{ kJ mol}^{-1}$  and this intermediate proved to be strongly bound to the surface, Figure 2c. The Cu-C bond is covalent, evidenced by the partial natural charges at copper and carbon atoms of  $+0.55$  and  $+0.37$ , respectively; the oxygen atoms originating from carbon dioxide bear a negative charge of  $-0.72$ . Carboxyl,  $-\text{CO}(\text{OH})$ , is considered as intermediate in the water-gas shift reaction (WGS,  $\text{CO} + \text{H}_2\text{O}$ ), and also in the reverse process (RWGS,  $\text{CO}_2 + \text{H}_2$ ).<sup>7,8,36</sup> The carboxyl has also been proposed as a key intermediate in methanol synthesis over copper catalysts from  $\text{CO}/\text{CO}_2/\text{H}_2/\text{H}_2\text{O}$  mixtures rather than formate ( $\text{HCOO}^*$ ).<sup>37</sup> The step to follow in the carboxyl route over metallic surfaces was suggested to be hydrogenation of the second oxygen atom to form carbene diol.<sup>37</sup> According to detailed DFT studies, the formate-to-formic acid reaction path was the energetically most favorable on metallic copper and on the commercial  $\text{Cu}/\text{ZnO}/\text{Al}_2\text{O}_3$  syngas to methanol catalyst.<sup>7,10</sup> Temperature-programmed reaction studies demonstrated that formate hydrogenation yields methanol over a  $\text{Cu}/\text{ZnO}/\text{Al}_2\text{O}_3$  catalyst,<sup>38</sup> but according to a more recent study bidentate binding of formate to the copper surface would prevent methanol synthesis; only the monodentate  $\text{HCOO}^*$  proved to be reactive, though not selectively, to methanol.<sup>37,39</sup> On  $\text{Cu}_2\text{O}$  however, though surface copper dimers play a key role in the hydrogenation, a different path is followed: our calculations indicate that the second hydrogenation step occurs at the carbon site and yields directly formic acid,  $\text{HCOOH}$ . The hydrogenation step to formic acid on the  $\text{Cu}_2\text{O}$  surface is endothermic by  $59.7 \text{ kJ mol}^{-1}$  and has a reaction barrier of  $121 \text{ kJ mol}^{-1}$ . The copper-oxygen bond bears some ionic character, with natural charge of  $+0.69$  at the copper center and  $-0.73 \text{ e}$  at the oxygen atom. The charge at the other oxygen atom forming the hydroxyl group is  $-0.67 \text{ e}$ . The role of formic acid in methanol synthesis from  $\text{CO}/\text{CO}_2/\text{H}_2$  has also been subject of debate – whether it is a reaction intermediate, or a byproduct.<sup>7,9</sup> The photocatalytic reduction of  $\text{CO}_2$  yielded formic acid among reaction products on a number of

semiconductor materials.<sup>21</sup> Our results for the reaction energetics compare well with the calculated data for metallic copper,<sup>7</sup> but while the adsorption energy of formic acid on metallic copper was calculated as very low, 21 kJ mol<sup>-1</sup>, on Cu<sub>2</sub>O the adsorption energy is much higher: 152 kJ mol<sup>-1</sup> on Cu<sub>14</sub>O<sub>7</sub> and 107 kJ mol<sup>-1</sup> on the Cu<sub>2</sub>O(001) nanolayer. The strongly adsorbed molecules of formic acid on Cu<sub>2</sub>O would rather participate in subsequent reduction, than being desorbed as side-product. The hydrogenation of formic acid to formaldehyde is weakly exothermic by 24 kJ mol<sup>-1</sup> and with a small energy barrier of 27.3 kJ mol<sup>-1</sup>. The transition state of this step corresponds to dihydroxymethylene species, H<sub>2</sub>C(OH)<sub>2</sub><sup>\*</sup> with one weakly bound hydroxyl group which is easily detached to a surface copper center, Figure 2e. A hydroxymethoxy intermediate has been considered in theoretical studies of the CO<sub>2</sub> hydrogenation mechanism over Cu/ZnO/Al<sub>2</sub>O<sub>3</sub> catalyst,<sup>9</sup> over pure metallic Cu,<sup>7</sup> but for a copper-ceria catalyst, recently reported as highly active in methanol synthesis from CO/CO<sub>2</sub>/H<sub>2</sub>, a formyl intermediate was suggested in the rate-determining step.<sup>9</sup> The main reason for the different reaction intermediates suggested for metallic, metal/oxide and oxide catalysts, is the stronger interaction between the oxide catalyst and carbon dioxide in the adsorption step, prior to hydrogenation. Surface carbonate, activated carbon dioxide CO<sub>2</sub><sup>δ-</sup>, and formate species were detected by IRRAS (Infrared Reflection-Absorption Spectroscopy) on Cu/CeO<sub>x</sub>.<sup>9</sup> While our results indicate that carbon dioxide undergoes bending upon adsorption at the Cu<sub>2</sub>O nanoclusters to form either surface carbonate or activated carbon dioxide (carboxylate-like, CO<sub>2</sub><sup>δ-</sup>), a formate intermediate is not formed on Cu<sub>2</sub>O – neither on finite clusters, nor at the nanolayers. Instead, further reduction of formaldehyde proceeds via strongly exothermic reaction to a methoxy intermediate, accompanied by water molecule release. The final step to methanol formation is weakly endothermic with a small energy barrier of 24 kJ mol<sup>-1</sup>, Figure 3. There is still high energy required for methanol desorption from the Cu<sub>2</sub>O surface as methanol molecules are attached by hydrogen bonds to the surface. The methanol adsorption energy on Cu<sub>2</sub>O compares well with the value calculated for a

Cu/CeOx catalyst ( $80 \text{ kJ mol}^{-1}$ ),<sup>9</sup> while on pure copper metallic surface it was calculated much smaller,  $27 \text{ kJ mol}^{-1}$ .<sup>7</sup>

The reaction balance requires oxygen evolution, as hydrogen from dissociated water molecules is consumed in the reaction. This step is usually the rate-determining one on oxide catalysts for water splitting.<sup>19,40-42</sup> The surface copper dimers provide a favorable site for the binding of the excess surface oxygen, which remains after the consumption of hydrogen. Peroxides and hydroperoxides are formed on copper surface dimers, Figure 4. The peroxide is weakly bound and dissociation of molecular oxygen requires  $47 \text{ kJ mol}^{-1}$ , Table 4. The hydroperoxo species, however, are more strongly bound to the surface. An activation barrier of  $130.5 \text{ kJ mol}^{-1}$  to peroxide formation from hydroperoxide was calculated. This energy barrier is higher, compared to the best known water splitting catalysts,<sup>19,20</sup> but it is not much higher than the highest energy barrier in CO<sub>2</sub> hydrogenation. The highest energy barriers calculated for the hydrogenation reaction and for oxygen evolution on Cu<sub>14</sub>O<sub>7</sub> appear in the red and near-IR region of the spectrum. In experimental studies, photocatalytic systems consisting of a co-catalyst and semi-conductor light harvester have been proposed in order to achieve efficient light absorbance for reaction activation.<sup>4,21,42</sup> As the reaction barriers of carbon dioxide reduction on Cu<sub>2</sub>O do not require high-energy activation, it is worthwhile to investigate the own light absorbance properties of the active phase. Time-dependent DFT calculations indicate that the Cu<sub>14</sub>O<sub>7</sub> cluster and the reaction intermediates have their most intense excitations in good agreement with the calculated activation energies, Table 5. In the adsorption complexes the excitations are slightly blue-shifted, most significantly in the carboxyl intermediate. The excitation energy of  $121 \text{ kJ mol}^{-1}$  needed for carboxyl-to-formic acid conversion falls in the near IR region (990 nm). The surface peroxide has intense absorption at 914 nm, which very well matches the activation barrier of  $130.5 \text{ kJ mol}^{-1}$  to peroxide formation. These results indicate that Cu<sub>2</sub>O nanoclusters would not require the use of supporting light harvesting material, because their own

absorptions could provide the energy needed for activation and for desorption of the final product, methanol.

## CONCLUSIONS

The surface stabilization of copper(I) oxide nanoclusters and nanolayers occurs via formation of Cu-Cu dimers and larger assemblies of copper cations. Upon adsorption of water or carbon dioxide, Cu-Cu bonds lengthen to allow binding of the adsorbate molecules. The carbon dioxide molecule undergoes strong bending upon adsorption. Water dissociation is spontaneous on the oxygen terminated Cu(001) surface, on  $\text{Cu}_{32}\text{O}_{16}$  and on a  $\text{Cu}_{14}\text{O}_7$  model cluster. The hydroxylated  $\text{Cu}_2\text{O}$  surface, resulting from water dissociation, provides hydrogen for  $\text{CO}_2$  reduction as bridging hydroxyl groups more easily donate hydrogen to the activated carbon dioxide molecules. The first step of hydrogenation is the formation of carboxyl group,  $-\text{CO}(\text{OH})$ , and this step is practically barrier free, with activation energy of  $13.8 \text{ kJ mol}^{-1}$ . The second hydrogenation step with formation of formic acid  $\text{HCO}(\text{OH})$ , requires activation energy of  $121 \text{ kJ mol}^{-1}$ . This barrier matches the maxima in light absorption of the  $\text{Cu}_{14}\text{O}_7$  clusters and the intermediate reaction products, which fall in the red to near IR region. The molecule of formic acid remains strongly adsorbed at the  $\text{Cu}_{14}\text{O}_7$  clusters and  $\text{Cu}_2\text{O}$  nanolayers, with adsorption energies of  $152 \text{ kJ mol}^{-1}$  and  $107 \text{ kJ mol}^{-1}$ , respectively. The strong binding of formic acid at the  $\text{Cu}_2\text{O}$  surface keeps it as a reactant for the next hydrogenation steps, to formaldehyde and methanol. Major advantage of  $\text{Cu}_2\text{O}$  over metallic catalysts is the strong interaction with  $\text{CO}_2$  and formic acid, which activates these molecules to undergo reduction. Methanol is also strongly bound to the surface via hydrogen bond formation, but less than the reaction intermediates.

**Acknowledgment.**

The computational results have been achieved using the Vienna Scientific Cluster (VSC). Special thanks are due to Dr. F. Clemente from Gaussian Inc. for his advice on periodic model calculations.

## SUPPLEMENTARY INFORMATION

Computational details, figures of large clusters, reaction intermediates formed on  $\text{Cu}_2\text{O}(001)$  nanolayers and Table 4S with calculated harmonic vibrational frequencies are presented as supplementary material (four pages).

## REFERENCES:

- (1) T. Sakakura, J.-C. Choi, and H. Yasuda *Chem. Rev.* 2007, **107**, 2365; A. J. Morris, G. J. Meyer, and E. Fujita *Acc. Chem. Res.*, 2009, **42**, 1983.
- (2) O. K. Varghese, M. Paulose, Th. J. LaTempa, C. A. Grimes *Nano Lett.*, 2009, **9**, 731.
- (3) G. Ghadimkhani, N. R. de Tacconi, W. Chanmanee, C. Janakyab and K. Rajeshwar *Chem. Commun.*, 2013, **49**, 1297.
- (4) G. Yin, M. Nishikawa, Y. Nosaka, N. Srinivasan, D. Atarashi, E. Sakai, and M. Miyauchi *ACS Nano*, 2015, **9**, 2111.
- (5) X.M. Liu, G.Q. Lu, Z.F. Yan, J. Beltramini, *Ind. Eng. Chem. Res.*, 2003, **42**, 6518.
- (6) G. A. Olah, A. Goepfert, G. K. S. Prakash, *Beyond Oil and Gas: The Methanol Economy*, 2<sup>nd</sup> edition; Wiley-VCH, Weinheim, 2009.
- (7) L. C. Grabow and M. Mavrikakis *ACS Catal.* 2011, **1**, 365
- (8) A. A. Gokhale, J. A. Dumesic, and M. Mavrikakis *J. Am. Chem. Soc.* 2008, **130**, 1402.
- (9) J. Graciani, K. Mudiyansele, F. Xu, A. E. Baber, J. Evans, S. D. Senanayake, D. J. Stacchiola, P. Liu, J. Hrbek, J. F. Sanz, J. A. Rodriguez, *Science*, 2014, **345**, 546.
- (10) M. Behrens, F. Studt, I. Kasatkin, S. Köhl, M. Hävecker, F. Abild-Pedersen, St. Zander, F. Girgsdies, P. Kurr, B.-L. Kniep, M. Tovar, R. W. Fischer, J. K. Nørskov, R. Schlögl *Science*, 2012, **336**, 893.
- (11) W. J. Durand, A. A. Peterson, F. Studt, F. Abild-Pedersen, J. K. Nørskov *Surface Science* 2011, **605**, 1354.

- (12) K. W. Frese Jr. *J. Electrochem. Soc.* 1991, **138**, 3338; (b) M. Le, M. Ren, Z. Zhang, P. T. Sprunger, R. L. Kurtz, and J. C. Flake, *J. Electrochem. Soc.* 2011, **158**, E45.
- (13) M. Hara, T. Kondo, M. Komoda, S. Ikeda, K. Shinohara, A. Tanaka, J. N. Kondo, K. Domen, *Chem. Commun.*, 1998, 357; P. E. de Jongh, D. Vanmaekelbergh, J. J. Kelly *Chem. Commun.*, 1999, 1069; K. E. R. Brown, K-S. Choi, *Chem. Commun.*, 2006, **31**, 3311. (d) S. Kakuta, T. Abe *Electrochem. and Solid-State Lett.*, 2009, **12**, P1.
- (14) C. R. A. Catlow, Z. X. Guo, M. Miskufova, S. A. Shevlin, A. G. H. Smith, A. A. Sokol, A. Walsh, D. J. Wilson, and S. M. Woodley, *Advances in computational studies of energy materials Phil. Trans. R. Soc. A* 2010, **368**, 3379; D. O. Scanlon, G. W. Watson, *Phys. Rev. Lett.*, 2011, **106**, 186403.
- (15) Z. Riguang, L. Hongyan, L. Lixia, L. Zhong, W. Baojun *Appl. Surf. Sci.* 2011, **257**, 4232
- (16) L. Y. Isseroff and E. A. Carter *Chem. Mater.* 2013, **25**, 253.
- (17) M. A. Nygren, L. G. M. Pettersson, A. Freitag, V. Staemmler, D. H. Gay, A. L. Rohl, *J. Phys. Chem.* 1996, **100**, 294.
- (18) M. A. Nygren, and L. G. M. Pettersson, *J. Phys. Chem.* 1996, **100**, 1874.
- (19) X. Li and P. E. M. Siegbahn *J. Am. Chem. Soc.* 2013, **135**, 13804.
- (20) M. W. Kanan, D. G. Nocera, *Science* 2008, **321**, 1072; D. G. Nocera, *Acc. Chem. Res.* 2012, **45**, 767; Y. Surendranath, M. W. Kanan, D. G. Nocera, *J. Am. Chem. Soc.* 2010, **132**, 16501.
- (21) S. C. Roy, O. K. Varghese, M. Paulose, and C. A. Grimes *ACS Nano*, 2010, **4**, 1259.

- (22) H. Raebiger, S. Lany, A. Zunger, *Phys. Rev. B* 2007, **76**, 045209; A. Soon, X-Y. Cui, B. Delley, S.-H. Wei, C. Stampfl, *Phys. Rev. B* 2009, **79**, 035205; D. O. Scanlon, G. W. Watson, *Phys. Rev. Lett.*, 2011, **106**, 186403.
- (23) K. H. Schulz, D. F. Cox, *Phys. Rev. B* 1991, **43**, 1610.
- (24) K. H. Schulz, D. F. Cox, *Surf. Sci.* 1991, **256**, 67.
- (25) O. Porat, I. Riess, *Solid State Ionics*, 1994, **74**, 229; O. Porat, I. Riess, *Solid State Ionics*, 1995, **81**, 29.
- (26) A. F. Izmaylov, G. Scuseria, and M. J. Frisch, *J. Chem. Phys.*, 2006, **125**, 104103; A. V. Krukau, O. A. Vydrov, A. F. Izmaylov, and G. Scuseria, *J. Chem. Phys.*, 2006, **125**, 224106.
- (27) Gaussian 09, Revision **D.01**, M. J. Frisch, G. W. Trucks, H. B. Schlegel, G. Scuseria, M. A. Robb, J. R. Cheeseman, G. Scalmani, V. Barone, B. Mennucci, G. A. Petersson, et al. Gaussian, Inc., Wallingford CT, 2009, see <http://gaussian.com>
- (28) A. D. Becke, *J. Chem. Phys.* 1996, **104**, 1040; A. D. Becke, *J. Chem. Phys.* 1993, **98**, 5648; C. Lee, W. Yang, R. G. Parr, *Phys. Rev. B*, 1988, **37**, 785; B. Miehlich, A. Savin, H. Stoll, H. Preuss, *Chem. Phys. Lett.* 1989, **157**, 200.
- (29) R. Bauernschmitt, R. Ahlrichs *J. Chem. Phys.*, 1996, **104**, 9047; R. Bauernschmitt, R. Ahlrichs *Chem. Phys. Lett.*, 1996, **256**, 454; F. Furche, R. Ahlrichs *J. Chem. Phys.*, 2002, **117**, 7433.
- (30) T. A. Halgren, W. N. Lipscomb, *Chem. Phys. Lett.*, 1977, **49**, 225; C. Peng, P. Y. Ayala, H. B. Schlegel, and M. J. Frisch, *J. Comp. Chem.*, 1996, **17**, 49.
- (31) S. Grimme, J. Antony, S. Ehrlich, H. Krieg, *J. Chem. Phys.*, 2010, **132**, 154104.

- (32) A. E. Reed, L. A. Curtiss, F. Weinhold, *Chem. Rev.* 1988, **88**, 899; F. Weinhold, J. E. Carpenter, *The Structure of Small Molecules and Ions*, (Plenum, 1988)
- (33) R. Restori, and D. Schwarzenbach, *Acta Cryst. B*, 1986, **42**, 201; W. Tiano, M. Dapiaggi, G. Artioli, *J. Appl. Cryst.*, 2003, **36**, 1461.
- (34) M. M. Islam, B. Diawara, V. Maurice, P. Marcus *Surf. Sci.* 2010, **604**, 1516; N. D. McClenaghan, P. Hu, Chr. Hardacre, *Surf. Sci.* 2000, **464**, 223.
- (35) S. Brahms, S. Nikitine, J. P. Dahl, *Phys. Lett.* 1966, **22**, 31; Z.-X. Shen, R. S. List, D. S. Dessau, F. Parmigiani, A. J. Arko, R. Bartlett, B. O. Wells, I. Lindau, and W. E. Spicer, *Phys. Rev. B* 1990, **42**, 8081.
- (36) D. B. Clarke, A. T. Bell, *J. Catal.* 1995, **154**, 314.
- (37) Y. Yang, C. A. Mims, D. H. Mei, C. H. F. Peden, C.T. Campbell, *J. Catal.* 2013, **298**, 10.
- (38) B. Sakakini, J. Tabatabaei, M. J. Watson, K. C. Waugh, F.W. Zemicael, *Farad. Discuss.* 1996, **105**, 369.
- (39) Y. Yang, C.A. Mims, R.S. Disselkamp, Ja-Hun Kwak, C.H.F. Peden, C.T. Campbell, *J. Phys. Chem. C* 2010, **114**, 17205.
- (40) Z. Fang, D. A. Dixon, *J. Phys. Chem. A*, 2013, **117**, 3539.
- (41) E. L. Uzunova, H. Mikosch *J. Chem. Phys.*, 2014, **141**, 044307.
- (42) A. Kudo, Y. Miseki, *Chem. Soc. Rev.*, 2009, **38**, 253.

**Table 1.** Lattice Constant ( $a$ , Å), Bond Lengths, Bond Angles, and Band Gap for  $\text{Cu}_2\text{O}$  as bulk crystal, thin layer  $\text{Cu}_2\text{O}$  (001), and nanocluster  $\text{Cu}_{32}\text{O}_{16}$ , calculated using the HSE06 functional and compared to experimental data.

	$a$ , Å	$R_{\text{Cu-O}}$ Å	$R_{\text{Cu-Cu}}$ Å	$\angle\text{CuCuCu}$ , deg	Direct gap, eV
$\text{Cu}_2\text{O}$ crystal	4.209	1.823	2.977		2.39
$\text{Cu}_2\text{O}$ (001) Cu-terminated	4.130	1.812 1.836 1.878	2.184 2.408 2.938	54.0; $2 \times 63.0$ ; 75.3	
$\text{Cu}_2\text{O}$ (001) O-terminated	4.130	1.721 1.836	2.478 2.939		
$\text{Cu}_2\text{O}$ (001) + ( $\text{H}_2\text{O}$ ) layer	4.206	1.794 1.841 1.861 2.137 <sup>a</sup> 2.000 <sup>b</sup>	2.887 2.934 3.015	55.3; $2 \times 62.2$ ; 78.0	
$\text{Cu}_2\text{O}$ crystal exp. <sup>c</sup>	4.267	1.84			2.17
$\text{Cu}_{32}\text{O}_{16}$			2.264 1.788 $\div$ 1.859 2.283 2.313 2.353	$2 \times 59.2$ 61.8 64.7	
$\text{Cu}_{14}\text{O}_7$		1.747 $\div$ 1.866	2.366 $\div$ 2.477	62.5 57.3 77.8 82.3	

<sup>a</sup>  $\text{Cu-O}_{\text{water}}$ ; <sup>b</sup>  $\text{Cu-O}_{\text{hydroxyl}}$ ; <sup>c</sup> experimental data from ref. 33 and 35

**Table 2.** HOMO-LUMO gaps (eV), natural population analysis and natural charges ( $q_M$ , e) of  $\text{Cu}_{32}\text{O}_{16}$  and  $\text{Cu}_{14}\text{O}_7$  clusters.

Cluster	HOMO-LUMO	$q_M$	$q_O$	M 3d	M 4s	O 2s	O 2p
$\text{Cu}_{32}\text{O}_{16}$	0.91	0.45-0.77	-1.07 ÷ -1.33	9.50÷9.72	0.48÷1.07	1.88÷1.90	5.15÷5.58
$\text{Cu}_{14}\text{O}_7$	0.63	0.51÷0.67	-1.06 ÷ -1.30	9.50÷9.70	0.75÷0.87	1.88÷1.91	5.14÷5.40

**Table 3.** Selected bond lengths before and after water dissociation on Cu<sub>2</sub>O nanolayer and clusters; enthalpy of surface hydroxyl group formation,  $\Delta H_{OH}$ .

	$R_{Cu-Cu}$ , Å before ads.	$R_{Cu-Cu}$ , Å after ads.	$R_{Cu-O}$ , Å before ads.	$R_{Cu-O}$ , Å after ads.	$R_{Cu-OH}$ , Å	$R_{OH}$ , Å	$\Delta H_{OH}$ , kJ mol <sup>-1</sup>
Cu <sub>2</sub> O (001), O terminated	2.478	2.976	1.721	1.794	2.000	0.963	144
	2.939	2.887				1.002	
Cu <sub>32</sub> O <sub>16</sub>	2.264	2.295	1.826	1.710	1.925	0.964	130
						1.041	
						1.482	
Cu <sub>14</sub> O <sub>7</sub>	2.450	2.567	1.951	1.880	1.868	0.965	174
						1.091	
						1.393	

Table 4. Reaction Activation Barriers ( $E_a$ ) and Binding Energies (BE) of Reaction Intermediates (in bold) for the Elementary Steps of  $\text{CO}_2$  Hydrogenation Using Water as a Source of Hydrogen, Calculated by B3LYP on a  $\text{Cu}_{14}\text{O}_7$  cluster. <sup>a</sup>

Reaction	BE, $\text{kJ mol}^{-1}$	$E_a$ , $\text{kJ mol}^{-1}$
$\text{H}_2\text{O} \Rightarrow \text{H}^{\bullet}_{\text{surf}} + \text{OH}^{\bullet}_{\text{surf}}$	156	0.9
$2 \text{OH}^{\bullet} \Rightarrow \text{H}^{\bullet}_{\text{surf}} + \text{OOH}^{\bullet}_{\text{surf}} \Rightarrow 2 \text{H}^{\bullet}_{\text{surf}} +$	336 <sup>b</sup>	130.5
$\text{O}_2(\text{ads})$	47 <sup>c</sup>	
$\text{CO}_2 + \text{O}^{\bullet\bullet}_{\text{surf}} \Rightarrow \text{CO}_3^{\bullet\bullet}_{\text{surf}}$	123	
$\text{CO}_2 + \text{Cu}_2^{\bullet\bullet}_{\text{surf}} + \text{O}^{\bullet\bullet}_{\text{surf}} \Rightarrow \text{CO}_2^{\delta-}_{\text{surf}} + \text{Cu}_2\text{O}^{\delta+}$	240	
$\text{CO}_2 + \text{H}^{\bullet} \Rightarrow \text{CO}(\text{OH})^{\bullet}$	395	13.8
$\text{CO}(\text{OH})^{\bullet} + \text{H}^{\bullet} \Rightarrow \text{HCO}(\text{OH})_{\text{surf}}$	152	121
$\text{HCO}(\text{OH})_{\text{ads.}} + \text{H}^{\bullet} \Rightarrow \text{H}_2\text{CO}_{\text{surf}} + \text{OH}^{\bullet}_{\text{surf}}$ via $\text{H}_2\text{C}(\text{OH})_2^{\bullet}$ as TS	85	27.3
$\text{H}_2\text{CO}_{\text{ads.}} + \text{H}^{\bullet} \Rightarrow \text{H}_3\text{CO}^{\bullet}_{\text{surf}}$	211	61
$\text{H}_3\text{CO}^{\bullet} + \text{H}^{\bullet} \Rightarrow \text{H}_3\text{C}(\text{OH})_{\text{surf}}$	127	24

<sup>a</sup> – vibrational frequencies of reaction intermediates are provided as Supplementary information, Table 4S; <sup>b</sup> – binding energy of hydroperoxide; <sup>c</sup> – binding energy of dioxygen adsorbed

**Table 5.** Maxima in the UV-VIS absorption spectra, calculated by TD DFT.

	Wavelength, nm	Oscillator strength
Cu <sub>14</sub> O <sub>7</sub>	821	0.03
	1070	0.05
Cu <sub>14</sub> O <sub>7</sub> with CO <sub>2</sub> adsorbed	798	0.04
	947	0.05
Cu <sub>14</sub> O <sub>7</sub> hydroxylated with CO <sub>2</sub> adsorbed <sup>a</sup>	995	0.06
Reaction intermediate Cu <sub>14</sub> O <sub>7</sub> with -CO(OH) adsorbed <sup>b</sup>	1060	0.03
	810	0.07
Reaction intermediate Cu <sub>14</sub> O <sub>7</sub> with H <sub>2</sub> C(OH) <sub>2</sub> <sup>c</sup> adsorbed <sup>d</sup>	898	0.03
	843	0.04
Cu <sub>14</sub> O <sub>7</sub> with surface hydroperoxide	914	0.03
Cu <sub>14</sub> O <sub>7</sub> with methanol adsorbed	886	0.03
	840	0.03

<sup>a</sup> Figure 2b <sup>b</sup> Figure 2c <sup>c</sup> Figure 2e

## Figure Captions

Figure 1. a) The  $\text{Cu}_2\text{O}$  unit cell. b) The  $\text{Cu}_{14}\text{O}_7$  nanocluster. c) The  $\text{Cu}_2\text{O}$  (001) copper-terminated surface with copper surface dimers and subsurface dimers denoted. d) The  $\text{Cu}_2\text{O}$  (001) oxygen-terminated surface with copper surface dimers denoted. Cu atoms are small red circles, O atoms – large blue circles.

Figure 2. The formation of a) surface carbonate species, b)  $\text{CO}_2$  adsorbed at two copper atoms, c) the carboxyl intermediate  $-\text{CO}(\text{OH})$  d) formic acid e) dihydroxymethylene intermediate  $\text{H}_2\text{C}(\text{OH})_2^*$  and f) methanol.

Figure 3. Elementary steps in the reaction path for  $\text{CO}_2$  hydrogenation to formic acid, with energy barriers and heat effects denoted. Blue arrows show desorption energies from the  $\text{Cu}_{14}\text{O}_7$  cluster, red arrows denote desorption from the nanolayer.

Figure 4. Surface peroxide (a) and hydroperoxide (b), formed after the hydrogen from hydroxyl groups was consumed in hydrogenation.

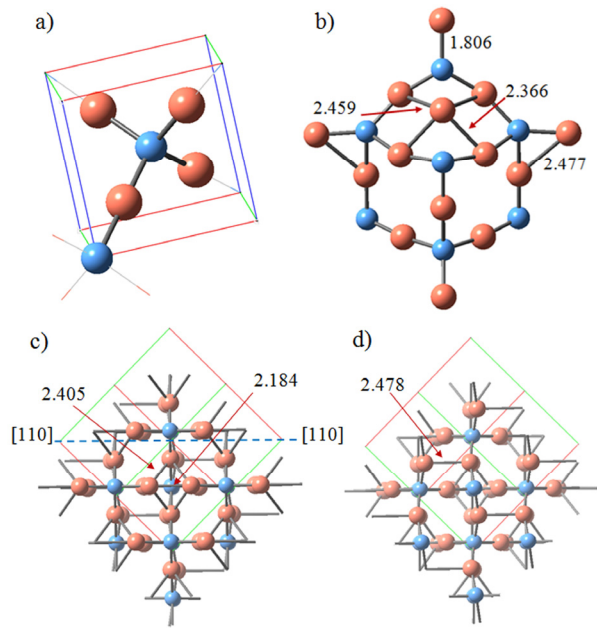


Figure 1

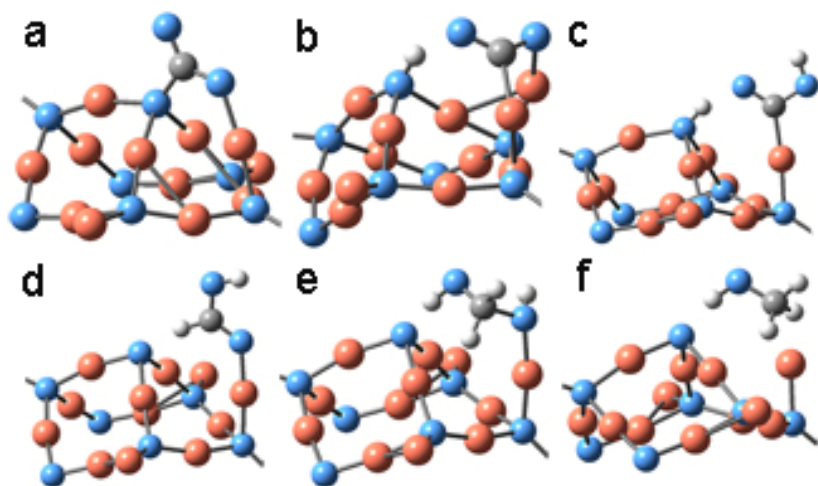


Figure 2

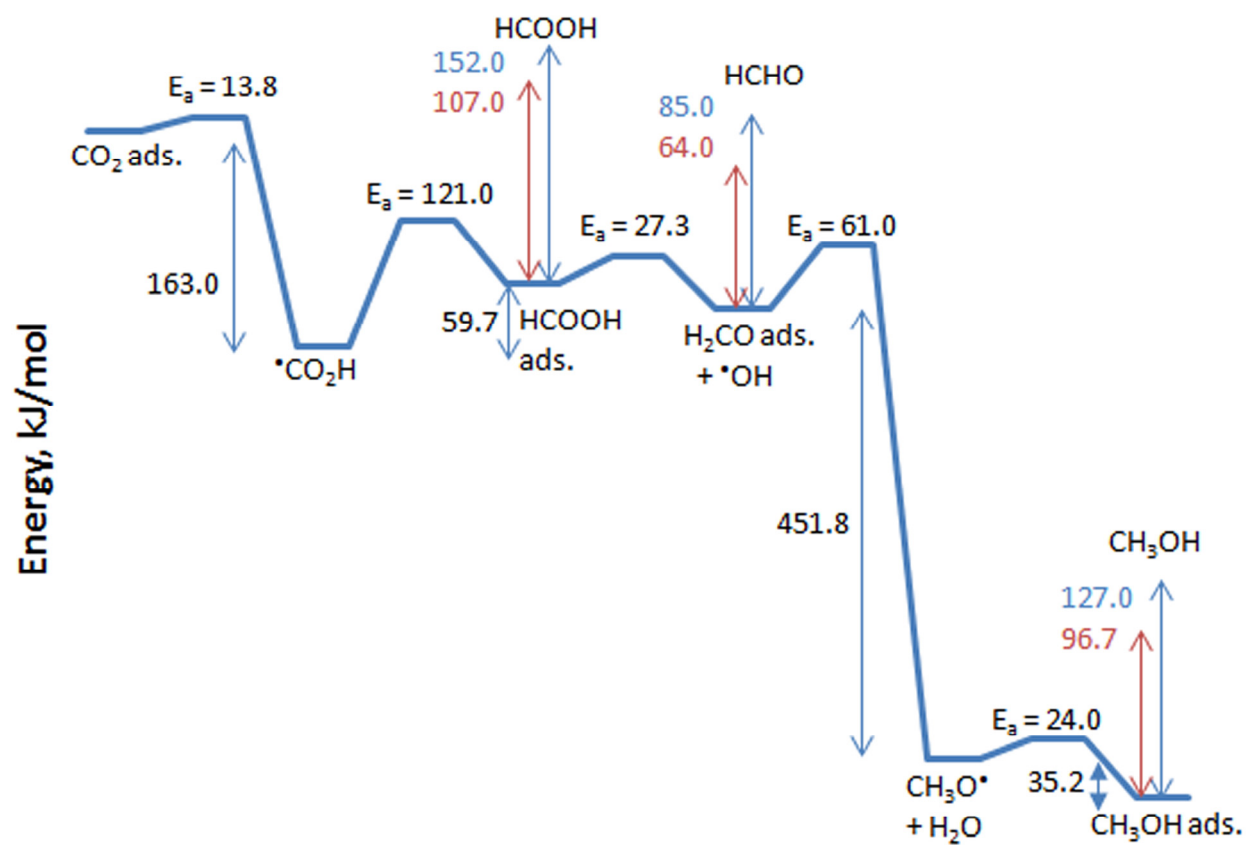


Figure 3

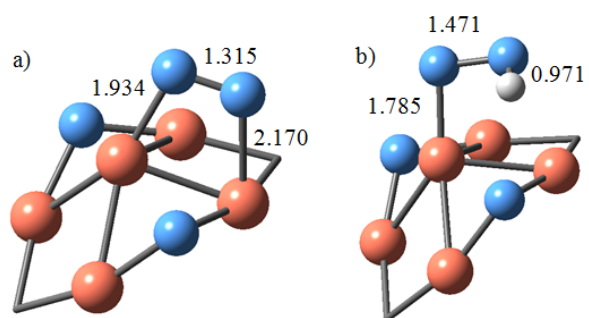
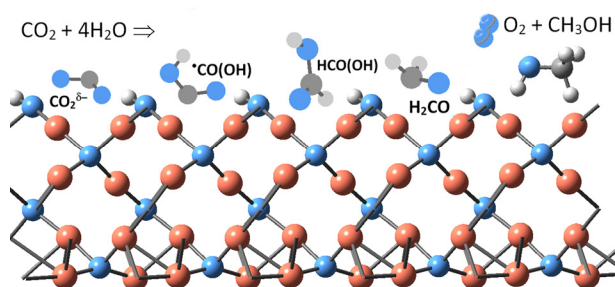


Figure 4

The CO<sub>2</sub> hydrogenation to methanol using dissociated water as hydrogen source proceeds via stable carboxyl, formic acid and formaldehyde intermediates.



Graphical abstract